How to cite: *Angew. Chem. Int. Ed.* **2021**, *60*, 11949–11958
International Edition: doi.org/10.1002/anie.202102183
German Edition: doi.org/10.1002/ange.202102183

VIP **Supramolecular Polymers** **Very Important Paper**

Polymorphism in Squaraine Dye Aggregates by Self-Assembly Pathway Differentiation: Panchromatic Tubular Dye Nanorods versus J-Aggregate Nanosheets

Chia-An Shen, David Bialas, Markus Hecht, Vladimir Stepanenko, Kazunori Sugiyasu,* and Frank Würthner**

In memory of Professor Siegfried Hünig

Abstract: *A bis(squaraine) dye equipped with alkyl and oligoethyleneglycol chains was synthesized by connecting two dicyanomethylene substituted squaraine dyes with a phenylene spacer unit. The aggregation behavior of this bis(squaraine) was investigated in non-polar toluene/tetrachloroethane (98:2) solvent mixture, which revealed competing cooperative self-assembly pathways into two supramolecular polymorphs with entirely different packing structures and UV/Vis/NIR absorption properties. The self-assembly pathway can be controlled by the cooling rate from a heated solution of the monomers. For both polymorphs, quasi-equilibrium conditions between monomers and the respective aggregates can be established to derive thermodynamic parameters and insights into the self-assembly mechanisms. AFM measurements revealed a nanosheet structure with a height of 2 nm for the thermodynamically more stable polymorph and a tubular nanorod structure with a helical pitch of 13 nm and a diameter of 5 nm for the kinetically favored polymorph. Together with wide angle X-ray scattering measurements, packing models were derived: the thermodynamic polymorph consists of brick-work type nanosheets that exhibit red-shifted absorption bands as typical for J-aggregates, while the nanorod polymorph consists of eight supramolecular polymer strands of the bis(squaraine) intertwined to form a chimney-type tubular structure. The absorption of this aggregate covers a large spectral range from 550 to 875 nm, which cannot be rationalized by the conventional exciton theory. By applying the Essential States Model and considering intermolecular charge transfer, the aggregate spectrum was adequately reproduced, revealing that the broad absorption spectrum is due to pronounced donor-acceptor overlap within the bis(squaraine) nanorods. The latter is also responsible for the pronounced bathochromic shift observed for the nanosheet structure as a result of the slip-stacked arranged squaraine chromophores.*

Introduction

Dye aggregates and color pigments provide the most striking examples for the emergence of new properties originating from *inter*molecular electronic couplings between molecular building blocks as a function of their supramolecular organization.[1] This interrelation is most evident for polymorphic states of a particular molecule, i.e., aggregates or solid state materials assembled by the same molecule in different packing arrangements. Whilst polymorphism in dye aggregates is still a rather new and accordingly less explored phenomenon, there is a long history of polymorphism in color pigments. Indeed, many of the commercially important colorants utilized as color pigments exist in different polymorphic forms with sometimes striking differences in color, shade, lightfastness, weather-fastness, dispersability, etc.[2] This is impressively highlighted by the most important industrial color pigment copper phthalocyanine (CuPc) for which meanwhile ten polymorphs have been identified. The most useful ones are the greenish blue β-form, which provide a perfect cyan shade for color printing applications, the reddish blue α-form used primarily in paints and the most reddish ε-form used in paints and blue color filters in LC displays.[3] Unsurprisingly, the performance of thin film transistors based on CuPc are also highly dependent on the packing arrangement accomplished by the respective processing conditions and the choice of the substrate.[4] Accordingly, CuPc pigments provide a perfect example how packing arrangements determine functional properties.

Compared to the mature field of color pigments, studies on polymorphism in dye aggregates are at the infant stage. Firstly, because the number of examples for polymorphic dye aggregates is still rather limited.[5,6] Secondly, because the packing arrangements in dye aggregates cannot be deter-

[*] C.-A. Shen, Dr. M. Hecht, Dr. V. Stepanenko, Prof. Dr. F. Würthner
Institut für Organische Chemie, Universität Würzburg
Am Hubland, 97074 Würzburg (Germany)
E-mail: wuerthner@uni-wuerzburg.de
Dr. D. Bialas, Dr. M. Hecht, Prof. Dr. F. Würthner
Center for Nanosystems Chemistry (CNC) and Bavarian Polymer Institute (BPI), Universität Würzburg
Theodor-Boveri-Weg, 97074 Würzburg (Germany)
E-mail: david.bialas@uni-wuerzburg.de
Prof. Dr. K. Sugiyasu
National Institute for Materials Science (NIMS)
1-2-1 Sengen, Tsukuba, Ibaraki 305-0047 (Japan)
E-mail: SUGIYASU.Kazunori@nims.go.jp
Supporting information and the ORCID identification number(s) for the author(s) of this article can be found under https://doi.org/10.1002/anie.202102183.

mined unambiguously like for their crystalline counterparts by single crystal X-ray crystallography and therefore correlations between structural and functional properties remain often rather speculative. Presumably the most profound studies in this regard exist for the class of perylene bisimide dye aggregates for which the impact of long-range Coulomb and charge transfer-mediated short-range coupling has been elaborated in depth and with this knowledge, packing arrangements could be deduced based on UV/Vis absorption spectra.[7]

This situation is, however, entirely different for squaraine dyes that constitute a most interesting class of dyes with regard to applications as they can provide cyanine-like intense and narrow absorption in the red part of the visible light spectrum along with strong fluorescence.[8] Furthermore, they show applicability as histological probes and in bioimaging,[9] excellent p-type semiconductivity in organic thin-film transistors[10] or solar cells,[11] giant circular dichroism in thin films,[12] as well as a plethora of sensing applications in supramolecular host-guest systems.[13] However, despite of this broad variety of applications, self-assembly of squaraines into dye aggregates remains less explored[14] and the relationship between packing structure and functional properties is often rather promiscuous for squaraine aggregates. Indeed, only most recently Spano and co-workers could unveil the origin of quite unusual absorption spectra of these dyes in thin films that strongly deviated from the expectations based on the common J- and H-aggregate molecular exciton model.[15]

Motivated by previous success in the non-covalent synthesis of structurally defined rod- and fiber-like dye aggregates by the self-assembly of suitably tethered bis-chromophores,[16] we recently initiated a research program to explore the supramolecular polymerization of bis(squaraine) dyes **BisSQ1** and **BisSQ2**, in which two dicyanomethylene squaraine chromophores are covalently linked either directly or via a phenylene spacer unit, respectively (Scheme 1). Aliphatic and hydrophilic side chains were attached to enhance microphase segregation. Interestingly, whilst **BisSQ1** self-assembly afforded only one type of dye aggregate that consists of a nanosheet structure with slip-stacked packing arrangement of the dyes and concomitant J-type exciton coupling,[17] our in-depth UV/Vis/NIR spectroscopic analysis of **BisSQ2** reveals the formation of two dye aggregate polymorphs with entirely different morphologies, i.e., nanorod and nanosheet, as well as optical properties, i.e., panchromatic and red-shifted absorption bands, respectively. Based on a combined effort by experimental work (microscopy and X-ray scattering) and theoretical calculations, we were able to derive reliable packing models for both polymorphs and to establish structure-function relationships. Most importantly, whilst the coloristic properties of the red-shifted nanosheet aggregate polymorph can be explained by the conventional molecular exciton model,[18] the panchromatic absorption spectrum for the tubular polymorph requires a more sophisticated treatment by the Essential States Model[19] taking into account *inter*molecular charge transfer interactions arising from the donor-acceptor overlap between the chromophores in the aggregated state.

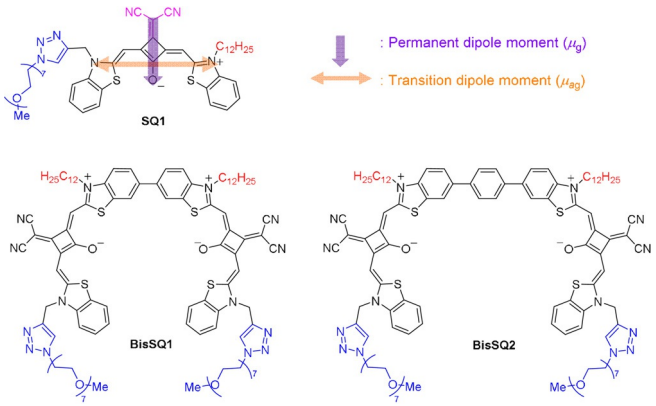

Scheme 1. Chemical structure of reference squaraine **SQ1** and bis(squaraine) dyes **BisSQ1**[17] and **BisSQ2** with graphical illustration of the orientation of the permanent and transition dipole moments, indicated by purple and orange arrow, respectively.

Results and Discussion

Synthesis and molecular properties

BisSQ2 was synthesized following the route shown in Scheme 2. Suzuki coupling reaction of compound **1**[17] with 1,4-benzenediboronic acid bis(pinacol) ester (**2**) afforded the target bis(squaraine) **BisSQ2**. The crude product was purified by recycling gel permeation chromatography (GPC) to give the pure **BisSQ2** in a yield of 23 %. For details on the synthetic procedures and characterizations of all new compounds, see the SI.

The absorption band of monomeric **BisSQ2** is broader and slightly red shifted ($\lambda_{max} = 726$ nm in $CHCl_3$, Figure S1c, green line) in comparison with the one of **SQ1** ($\lambda_{max} = 703$ nm), which is attributable to the conformational flexibility due to the rotation around the phenyl-phenyl bonds in the spacer unit. Hence, various mutual arrangements of the chromophores exist in solution, which in turn leads to different electronic interactions, and thus a broadening of the absorption band.[20] Like that of **SQ1**, fluorescence spectrum of **BisSQ2** exhibits a small Stokes shift (260 cm^{-1}) and a mirror image behavior with its absorption spectrum (Figure S2b). However, a significant decrease in the fluorescence quantum yield to 42 % and a reduced fluorescence lifetime of 3.01 ns in comparison to **SQ1** (79 % and 4.78 ns, respectively) are

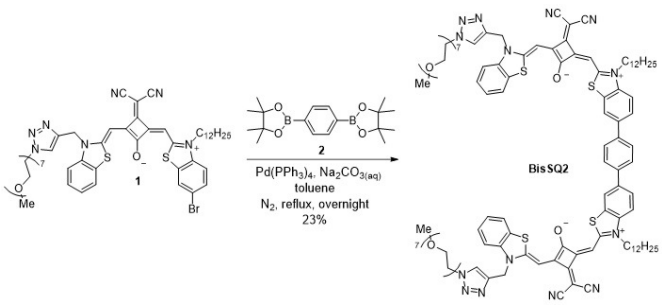

Scheme 2. Synthesis of bis(squaraine) **BisSQ2**.

observed. Our analysis of radiative (k_{fl}) and non-radiative (k_{nr}) decay constants suggests a more effective non-radiative decay originating from the conformational flexibility in **BisSQ2** (Table S1). It is noteworthy that the excitation spectrum of **BisSQ2** resembles the absorption spectrum (Figure S2b), which indicates that the various emissive states resulting from the different conformations are close in energy.

Self-assembly into supramolecular polymers

In order to trigger *inter*molecular aggregation driven by dispersion and dipolar interactions, solvents with low polarity are required.[21] Therefore, we have performed aggregation studies for **BisSQ2** in a solvent mixture of toluene/1,1,2,2-tetrachloroethane (TCE) = 98:2 (*v*/*v*). TCE was used as an additive to increase the solubility of **BisSQ2** in order to cover a broad concentration range. The sample solution was prepared by dissolving **BisSQ2** in TCE first and then diluting with toluene. After heating the as-prepared solution (toluene/TCE 98:2, $c = 2.5 \times 10^{-5}$ M) to 85 °C for 20 minutes to achieve a fully monomeric state (Figure 1, gray dashed curve) and cooling it down to 25 °C, different spectral features are observed depending on the cooling rate. Rapid cooling, i.e., transferring the hot solution immediately into a pre-cooled chamber at 25 °C, leads to the formation of a broad band feature with absorption maxima at 605, 737, and 783 nm (Figure 1, blue curve); hereafter, this aggregate is denoted as **BisSQ2-AggI**. In contrast, slow cooling (cooling rate = 2 °C min^{-1}) apparently resulted in a different outcome as suggested by the formation of precipitates. To disperse the precipitates, we applied sonication and measured its absorption spectrum: a bathochromically shifted sharp absorption band ($\lambda_{max} = 780$ nm, $FWHM = 420$ cm^{-1}) with respect to the monomeric state ($\lambda_{max} = 739$ nm) was observed (Figure 1, red curve). This result indicates the formation of J-type aggregates, which we refer to as **BisSQ2-AggII**. We note that a similar spectrum was observed for a solution before the sonication, although absorbance was smaller because of the precipitation (Figure S5b, blue curve). Thus, we infer that the applied sonication does not lead to dissociation or a new aggregate species.[5a,d,22] The distinct absorption spectra indicates that a supramolecular polymorphism occurs depending on the cooling rate.

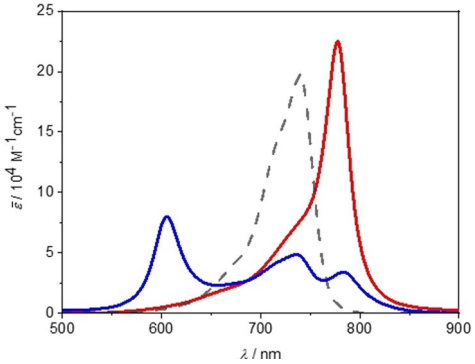

Figure 1. UV/Vis/NIR spectra of a solution of **BisSQ2** ($c = 2.5 \times 10^{-5}$ M, toluene/TCE 98:2) at 85 °C (gray) and those at 25 °C obtained upon rapid cooling (blue: **AggI**) and slow cooling (red: **AggII**). Because precipitation happened during the sample preparation by slow cooling, ultra-sonication was applied for 20 minutes to the solution to disperse the precipitate prior to the measurement.

Structural insights and packing model

To gain deeper insight into the structural features of the **BisSQ2** aggregates, atomic force microscopy (AFM) measurements were performed. A solution of **BisSQ2-AggI** in toluene/TCE (98:2, *v*/*v*) with a concentration of 2.5×10^{-5} M was spin-coated onto a silica wafer (SiO_x); we observed stiff helical rod-like aggregates with lengths up to 1.5 μm, a well-defined diameter of 5.0 ± 0.2 nm, and both left- (*M*) as well as right- (*P*) handedness (Figure 2 a–c). The helical pitch was measured to be 13 ± 1 nm (Figure 2 d). These results suggest the presence of a complex internal structure consisting of multiple **BisSQ2** units to form the nanorods.[23]

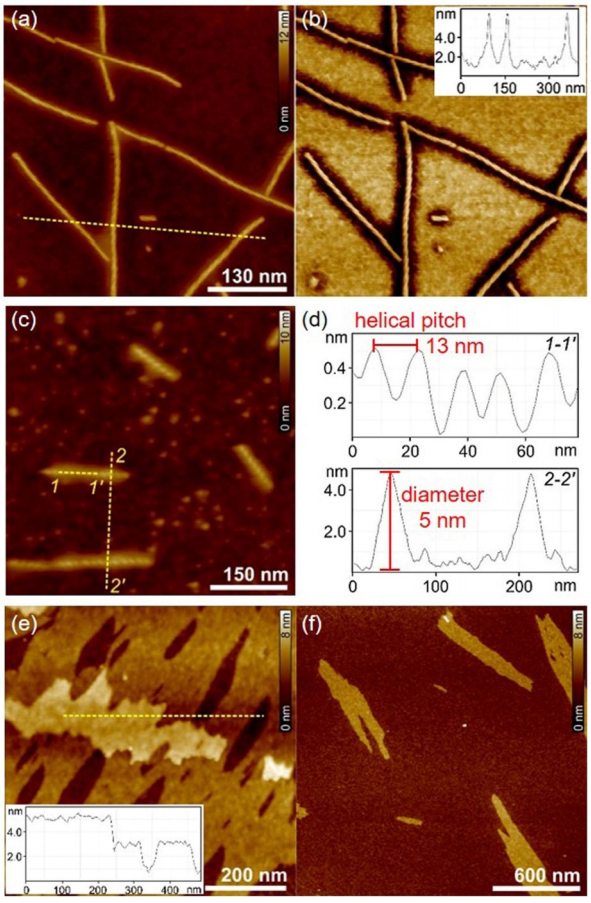

Figure 2. a) Height (*Z* scale = 12 nm) and b) phase AFM images of **BisSQ2-AggI**; inset: the cross-section analysis from yellow dashed line in image (a). c) Height (*Z* scale = 10 nm) AFM image of **BisSQ2-AggI**. d) Cross-section analyses from the yellow dashed lines 1-1′ and 2-2′ in image (c). e) Height AFM image of **BisSQ2-AggII**; inset: the cross-section analysis from yellow dashed line in image (e). f) Height AFM image of **BisSQ2-AggII** (solution sonicated for 30 s). *Z* scale is 8 nm for both (e) and (f). All samples for AFM measurements were prepared by spin-coating of toluene/TCE 98:2 solutions of **BisSQ2** ($c = 2.5 \times 10^{-5}$ M) on SiO_x with 2000 rpm.

Interestingly, **BisSQ2-AggII** showed a significantly different morphology. Multi-layers of two-dimensional sheet-like structures with height of 2.1 ± 0.2 nm and widths up to 1 μm are observed (Figure 2e). Such large-sized aggregates are in line with the observation of the precipitation. We have also performed AFM studies on the **BisSQ2-AggII** solution that was treated by ultra-sonication for 30 seconds. Similar sheet-like structures are visible on the substrate (Figure 2f), corroborating that sonication can fragment the precipitates into small pieces and disperse them in solution but does not change the aggregation mode of **BisSQ2**.

To gain further information about the aggregate structure, X-ray scattering techniques were applied. A thick film was prepared on aluminum foil by slow evaporation of a concentrated solution of **BisSQ2-AggI** ($5\,g\,L^{-1}$ in toluene/TCE = 98:2). Figure 3a depicts the wide and small angle X-ray scattering (WAXS and SAXS) diagram of the film. The diffuse halo in the wide-angle region corresponds to the liquid-like disordered structure of the surrounding alkyl chains. The observed peaks indicate a hexagonal columnar arrangement of rods in the solid state with an *inter*columnar distance of 6.22 nm, which is in good agreement with the rod diameter of 5 nm as determined by AFM measurements (Figure 2d). In contrast, for a thick film drop-casted from a concentrated solution of **BisSQ2-AggII** onto an aluminum foil, the X-ray scattering diagram shows a completely different pattern. Equidistant signals can be observed (labelled as 001-004 in Figure 3b). This hints toward a lamellar arrangement with a layer distance of 2.32 nm, in accordance with the layer thickness of 2.1 nm obtained from AFM (Figure 2e).

The experimental data obtained from AFM and WAXS measurements enable us to derive packing models for the two different types of aggregates. For **BisSQ2-AggI**, we propose a nanorod structure as displayed in Figure 3c, in which nine **BisSQ2** molecules form one turn of a helical supramolecular polymer chain (pitch of 11 nm, highlighted in red) with a diameter of 4 nm (Figure 3c and Figure S6). Assuming a reasonable density of $1\,g\,cm^{-3}$ for soft organic materials,[24] the number of molecules per repeating unit amounts to 72 molecules (see SI). This corresponds to eight helically wound strands that intertwine to form the tubular rod-shaped supramolecular polymer structure presented in Figure 3c, where each strand is colored individually. According to this model, the aliphatic chains are closely packed inside the nanorods (Figure 3c top view, green part), while the hydrophilic OEGs point to the outside of the nanorods (blue part), exhibiting an ideal phase segregation. An opposite orientation of the side-chains, i.e., the OEGs point to the inside and the aliphatic side chains to the outside of the nanorod, does not result in a reasonable structure that is consistent with the experimental data. Similar structural arrangements, where OEGs are found on the outer surface, were described for self-assembled nanotubes composed of hexabenzocoronene amphiphiles in toluene.[25] Considering the side chains, the dimensional parameters are in good accordance with the experimental results. A closer look at the chromophores reveals a sandwich-type arrangement with antiparallel orientation of the ground state dipole moments (Figure 3c, cut-out comprising two chromophores colored in red). Remarkably, the chromophores are arranged in a slipped fashion, where the donor parts are in close proximity to the acceptors of the neighboring molecules.

The morphology of **BisSQ2-AggII** revealed by our AFM studies resembles the nanosheet structure observed for

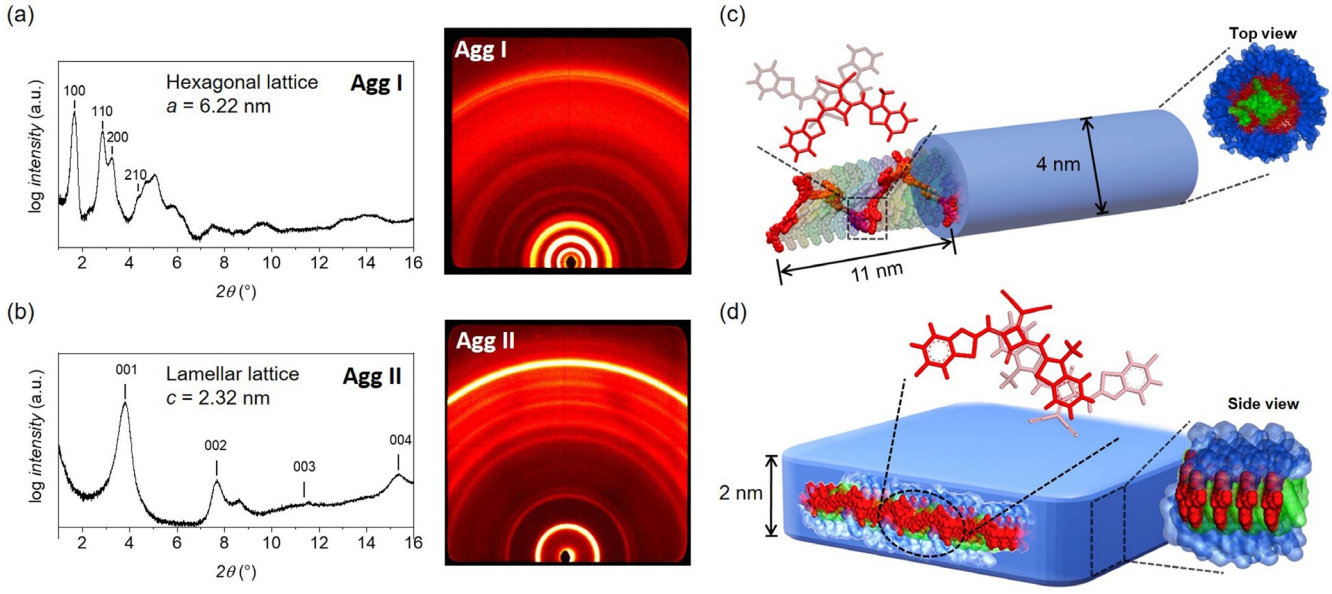

Figure 3. WAXS measurements of a) **BisSQ2-AggI** and b) **BisSQ2-AggII** prepared on aluminum foils by multistep evaporation of the respective solutions (toluene/TCE 98:2, $c = 5.0\,g\,L^{-1}$) and proposed packing model of (c) the tubular nanorod of self-assembled **BisSQ2-AggI**; left: each strand individually colored (side chains omitted), showing a cut-out of a helix comprising two chromophores, which shows a close spatial proximity between donor and the acceptor of the adjacent chromophore; right: top view with hydrophilic side chains (blue) and aliphatic chains (green); d) the nanosheet of self-assembled **BisSQ2-AggII** with the chromophores colored in red, hydrophilic side chains in blue and the aliphatic chains in green, respectively. Both models were simulated and visualized with the program suite *BIOVIA Materials Studio 2017R2*.

bis(squaraine) dye **BisSQ1** (Scheme 1) in our earlier work,[17] for which a slipped-stack arrangement between neighboring chromophores was proposed. This is further supported by the observed red-shifted absorption spectrum (Figure 1, red line), indicating a head-to-tail arrangement of the chromophores with J-type coupling[18] (Figure 3d and Figure S7). The alkyl side chains (Figure 3d, green) accommodate themselves in the hydrophobic cavities between the chromophores, while the polar OEG chains (Figure 3d, blue) extend above and below the sheet into the solvent. The observed height of 2.1 nm by AFM is in good agreement with the dimension of the chromophore considering the flexibility of the side chains (Figure S8a), suggesting the formation of a monolayer on the substrate.

Concentration-dependent UV/Vis/NIR spectroscopy

To gain more insight into the aggregation mechanism of **BisSQ2**, concentration-dependent UV/Vis/NIR studies were carried out. A stock solution (toluene/TCE 98:2, $c = 1.8 \times 10^{-4}$ M) of **BisSQ2-AggI** was prepared by the fast-cooling method as mentioned above. For detailed methods for sample preparation, see the SI.

This **BisSQ2-AggI** stock solution was then diluted into a series of samples with a concentration range of 1.8×10^{-4}–6.0×10^{-7} M and all sample solutions were equilibrated at room temperature for 24 hours prior to the measurements. At high concentration ($c = 1.8 \times 10^{-4}$ M), a broad absorption band characteristic of **BisSQ2-AggI** was observed (Figure 4a, blue line). Upon decreasing the concentration, pronounced spectral changes are visible, revealing dissociation of the aggregates. At low concentration (Figure 4a, red line), the absorption spectrum exhibits a rather sharp band at $\lambda_{max} =$ 739 nm, which resembles the monomer absorption spectrum observed at high temperatures (see Figure 1). Notably, isosbestic points are observed at 656 and 766 nm, indicating an equilibrium between only two species. The abrupt change of the apparent absorption at 739 nm (Figure S10a) at a critical concentration of $c_T \approx 4 \times 10^{-6}$ M indicates a cooperative aggregation process.[26] Hence, we made use of the cooperative K_2/K model, where two states of the aggregation process are differentiated: the nucleation regime, described by the equilibrium constant K_2 for the dimerization, and the elongation regime, described by the equilibrium constant K.[27] The data could be properly fitted (Figure 4a, inset) to give a cooperativity factor $\sigma = 0.016$ with $K = 2.18 \times 10^5$ M^{-1} for the elongation regime, resulting in an equilibration constant for the dimerization of $K_2 = 3.56 \times 10^3$ M^{-1}. It is noteworthy that the isodesmic (equal-K) model ($\sigma = 1.0$) and monomer-dimer model both failed to describe the aggregation process (Figure S10a). The high cooperativity suggests that only a small number of nuclei are involved in the equilibrium and mainly monomers and extended aggregates are present in the solution over the whole concentration range, which is in agreement with the appearance of the isosbestic points in the concentration-dependent spectral changes (Figure 4a). By applying a global fit analysis[28] (for further details, see the SI), the ideal monomer and aggregate spectra were obtained, which match perfectly with the spectra obtained for the most diluted and most concentrated solutions, respectively (Figure 4a, red and blue solid lines). The aggregate spectrum exhibits a remarkable broad absorption covering the whole range of 550–850 nm, edging in the NIR region. The absorption features do not allow us to gain insight into the chromophore arrangement in terms of a simple classification of H- (sandwich type arrangement) and J-aggregates (head-to-tail arrangement),[18] which will be discussed later.

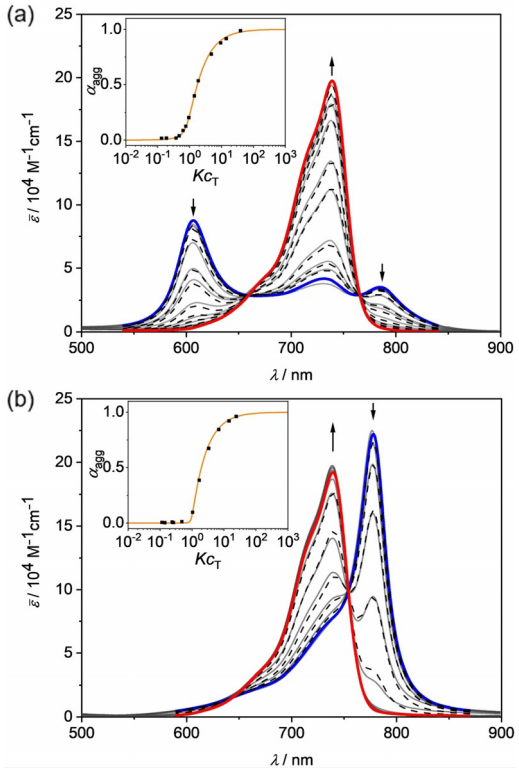

Figure 4. Concentration-dependent UV/Vis/NIR spectra of **BisSQ2** (a) AggI ($c = 1.8 \times 10^{-4}$–6.0×10^{-7} M) and (b) AggII ($c = 3.8 \times 10^{-5}$–1.8×10^{-7} M) in toluene/TCE 98:2 at 25 °C (grey solid lines) and the global fit analysis according to the cooperative K_2/K model[27] (black dashed lines) and the ideal monomer (red solid line) as well as aggregate spectra (blue solid line) obtained by global fit analysis. The arrows indicate the spectral changes with decreasing concentration. Inset: plot of fractions of aggregate against Kc_T and fit with the cooperative K_2/K model[27] (c_T is the total concentration of **BisSQ2** molecules in solution).

For **BisSQ2-AggII**, since precipitation took place after the cooling process, we prepared a fresh **BisSQ2-AggII** solution (toluene/TCE 98:2, $c = 3.8 \times 10^{-5}$ M) and applied ultra-sonication at 25 °C for 20 minutes to disperse the aggregates. The solution was further diluted stepwise to obtain a series of samples with different concentrations. The sample solutions were stored overnight prior to the measurements. Upon dilution, the aggregate band decreases accompanied by the growth of the monomer band peaked at 739 nm with a FWHM of 540 cm^{-1} (Figure 4b). As in the case of **BisSQ2-AggI**, a defined isosbestic point can be observed at 754 nm, suggesting an equilibrium between only two species.

The results again infer a cooperative aggregation process (Figure S10b), therefore, we applied the cooperative K_2/K model[27] (Figure 4b, inset) that delivered a cooperativity factor $\sigma = 0.00038$ with $K = 6.37 \times 10^5\ M^{-1}$ for the elongation regime, resulting in an equilibrium constant for the dimerization of $K_2 = 2.42 \times 10^2\ M^{-1}$. Again, the isodesmic (equal-K) model ($\sigma = 1.0$) and monomer-dimer model failed to describe the aggregation process (Figure S10b). This result reveals a higher cooperativity as well as a larger elongation constant for the aggregation process of **BisSQ2-AggII** compared with **BisSQ2-AggI** ($\sigma = 0.016$, $K = 2.18 \times 10^5\ M^{-1}$), suggesting that **BisSQ2-AggII** is the thermodynamically favored species. The resulting ideal aggregate spectrum (Figure 4b, blue solid line) obtained by global fit analysis[28] (for further details, see the SI) shows a significant red-shift and sharpening compared to the monomer spectrum (Figure 4b, red solid line). In addition, the aggregate spectrum also shows weak side-bands at higher energies, i.e., shorter wavelengths.

We also performed temperature-dependent UV/Vis/NIR experiments for **BisSQ2-AggII** solution (toluene/TCE 98:2, $c = 2.5 \times 10^{-5}$ M). Even though quantitative analysis of the spectra is not possible due to precipitation, the results suggest that heating leads to the dissociation of **BisSQ2-AggII** directly into monomers without showing absorption features of **BisSQ2-AggI** (Figure S11). Combining this observation with our concentration-dependent kinetic analyses (Figure S13), we infer that **BisSQ2-AggI** is an off-pathway species and **BisSQ2-AggII** the thermodynamically more stable aggregate.[29] Based on these results, we deduce the energy landscape shown in Figure 5 that depicts the two competing self-assembly pathways qualitatively. At high temperature (85 °C), **BisSQ2** molecules remain dissociated. Upon rapid cooling, the aggregation follows the pathway with the lowest energy barrier (solid arrow in Figure 5) and ends up in a kinetically trapped state: i.e., **BisSQ2-AggI**. According to the proposed model shown in Figure 3c, the arrangement of the side chains reveals a phase segregation that may contribute to the low energy barrier of the self-assembly process.[30] In contrast, during the slow cooling process, the system has a time long enough to traverse the energy landscape and find a more stable and well-organized aggregation mode (dotted arrows in Figure 5): as a consequence, **BisSQ2-AggII** is formed.

Polymorphisms in supramolecular polymerization have been observed for monomers bearing multiple non-covalent interaction sites. Prominent examples are benzene-1,3,5-tricarboxamide molecules (BTAs) whose regular self-assembly into 1D fibers[31] was transformed into 2D and 3D morphologies by additional H-bonding interactions by shielding carboxyl groups in a hydrophobic environment[5b] or by alteration of the alkyl chain length for porphyrin molecules, likewise transforming the self-assembly into 1D fibers[5a] by increasing the lateral van der Waals forces to afford a 2D sheet-like morphology. In this context, it is intriguing that we observed polymorphism for **BisSQ2**, but not for **BisSQ1** despite of the absence of specific measures as described above for the BTAs and alkyl porphyrins.[17] Both molecules consist of two squaraine dyes connected in the same angle. It appears that the additional spacer between the squaraine dyes in **BisSQ2** allowed another form of folding and packing (i.e., **BisSQ2-AggI**), which demonstrates a new strategy to realize supramolecular polymorphism. Remarkably, as discussed below, a hitherto unknown panchromatic absorption spectrum, i.e., modulation of the functional properties, was achieved by this simple strategy.

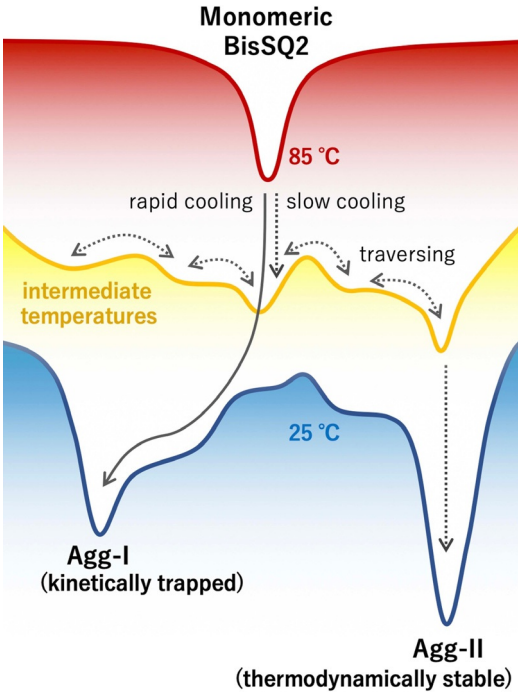

Figure 5. Schematic energy landscape of the two competing pathways for the formation of kinetically favored off-pathway **BisSQ2-AggI** and the thermodynamically more stable **BisSQ2-AggII** in toluene/TCE 98:2. Upon rapid cooling, **BisSQ2-AggI** is formed and kinetically trapped. Note that **BisSQ2-AggI** has less organized structure (Figure 3), thus is kinetically more favored. In contrast, during the slow cooling process, **BisSQ2** has a time long enough to traverse the energy landscape and find a more stable and well-organized aggregation mode.

Theoretical calculations for dye-dye interactions

Since the discovery of J-aggregates by Jelley and Scheibe,[32] scientists were interested to understand how supramolecular arrangements govern dye-dye interactions and how these interactions manifest in absorption spectra and determine functional properties. This is perfectly demonstrated by Kasha's molecular exciton theory that had a great impact on research on dye aggregates and functional molecular materials for more than 50 years.[18] In this regard, it is most interesting that the absorption features of the **BisSQ2-AggI** cannot be explained for the chromophore arrangement deduced from X-ray analysis in terms of a simple classification of H- (sandwich type arrangement) and J-aggregates (head-to-tail arrangement) by the molecular exciton theory. Based on this model, we would expect a hypsochromic shift (H-aggregate) of the main absorption peak with respect to the monomer according to the packing model shown in Figure 3c, rather than a panchromatic absorption as observed for

BisSQ2-AggI.[18] Transitions to both the highest and lowest excited states can be allowed in case of a rotational displacement of the chromophores resulting in the appearance of a weaker J-band in the absorption spectrum (Davydov splitting).[33] However, this would require a large rotational angle in our case since both bands show significant intensity (Figure 4a, blue solid line).[20b] For such a situation, however, only small shifts are expected which is obviously not the case for the **BisSQ2-AggI** nanorods.

Hence, in order to understand the broad panchromatic absorption spectrum of **BisSQ2-AggI** nanorods and also rationalize the bathochromic shift observed for **BisSQ2-AggII** nanosheets, we applied the Essential States Model (ESM).[19] In contrast to conventional molecular exciton theory, this model also accounts for polarizability effects, being crucial for the description of the optical properties of dye aggregates comprising chromophores composed of alternating donor and acceptor subunits.[34,35] Squaraines exhibit a significant charge transfer character arising from *intra*molecular transfer of electron density from the donor to the acceptor moiety within the donor-acceptor-donor chromophore. Thus, the squaraine chromophore is described by three essential states: two zwitterionic states $|Z_1\rangle$ and $|Z_2\rangle$ bearing a positive charge at one of the donor units and a negative charge at the acceptor moiety, respectively, which are both coupled to the neutral state ($|N\rangle$) by the transfer integral t_Z (Figure 6a).[36] The respective electronic Hamiltonian can be written as[36]

$$\hat{H}_{el}^{mon} = \eta_Z \sum_{i=1,2} |Z_i><Z_i| + t_Z \sum_{i=1,2} (|N><Z_i| + h.c.), \quad (1)$$

with η_Z being the energy of the zwitterionic states (note that the energy of the neutral state is set to zero) and *h.c.* the Hermitian conjugate. In order to account for vibronic coupling, as evident from the vibronic progression observed in the UV/Vis/NIR spectrum of **SQ1**, we employed a Holstein-type Hamiltonian (for details see the SI). Thereby, each essential state is described by two harmonic oscillators, that is, one for each donor-acceptor side arm. In doing so, the UV/Vis/NIR spectrum of reference dye **SQ1** is well reproduced by our simulation (Figure S15, blue solid line) using the parameters shown in Table S2, which are in line with previous studies on squaraine dyes.[20b] The zwitterionic character ρ in the ground state is given by equation (2).[36]

$$\rho = \frac{1}{2}\left(1 - \frac{\eta_Z}{\sqrt{\eta_Z^2 + 8t_Z^2}}\right). \quad (2)$$

In this way, we obtain a value of $\rho = 0.46$ revealing an almost equal contribution of the neutral and zwitterionic states (note that a fully zwitterionic character results in $\rho = 1$, whereas a completely neutral state is characterized by $\rho = 0$). This explains the observation of a sharp cyanine-like absorption band with a weak vibronic side-band (Figure S15, blue solid line and Figure S1c, black line).

Having set the parameters for the monomeric chromophore, we simulated the absorption spectrum for a cut-out of **BisSQ2-AggI** nanorod comprising the two chromophores

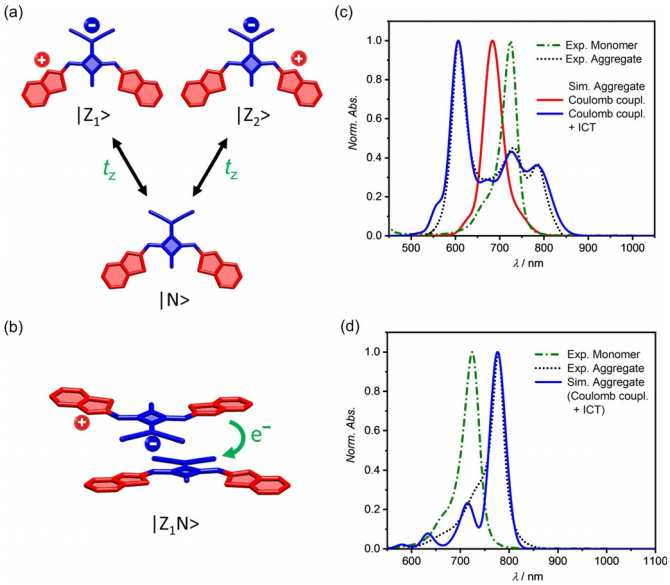

Figure 6. a) Three diabatic states used for the simulation of the absorption spectrum of **SQ1** monomer and **BisSQ2** aggregates. The zwitterionic states $|Z_1\rangle$ and $|Z_2\rangle$ are characterized by a positive and negative charge at the donor and acceptor moiety highlighted in red and blue, respectively. Both states are coupled to the neutral state $|N\rangle$ by the transfer integral t_Z describing the *intra*molecular electron transfer from the donor to the acceptor unit. b) Schematic representation of the *inter*molecular electron transfer in the double squaraine stack of **BisSQ2-AggI** in state $|Z_1N\rangle$. Simulated absorption spectrum of the double chromophore stack of (c) **BisSQ2-AggI** and (d) **BisSQ2-AggII** taking Coulomb coupling and *inter*molecular charge transfer states (ICT) into account (blue solid lines). In addition, the simulated spectra of **BisSQ2-AggI** considering only Coulomb coupling (red solid line) is shown in panel (c). The experimental spectra of the aggregates (black dotted lines, toluene/TCE 98:2) and the monomer (green dash-dotted lines) are also shown for comparison. For the simulations, the parameters listed in Table S2 were employed. The calculated spectra (blue lines) were shifted by 200 cm^{-1} (**BisSQ2-AggI**) and −500 cm^{-1} (**BisSQ2-AggII**).

shown in Figure 3c to reduce computational effort. Even though this is a simplification, it allows us to investigate the origin of the broad absorption spectrum of **BisSQ2-AggI**. Toward this approach, we first evaluated the influence of the Coulomb coupling between the chromophores (for a detailed description see the SI). Using the same parameters as for the monomer (Table S2), the resulting absorption spectrum due to Coulomb coupling shows a main absorption band (Figure 6c, red solid line) with a hypsochromic shift compared to the monomer absorption band (green dash-dotted line). This is in agreement with a sandwich-type cofacial arrangement of the chromophores resulting in H-type exciton coupling.[18] Hence, it is obvious that the broad absorption spectrum of **BisSQ2-AggI** (Figure 6c, black dotted line) and in particular the pronounced absorption in the NIR-region cannot be rationalized by considering only Coulomb coupling between the chromophores because the shift is too small and no second J-band due to Davydov splitting is present.

However, our modelling studies reveal close spatial proximity of the donor and acceptor groups (Figure 3c), which suggests the importance of *inter*molecular charge

transfer (ICT, Figure 6b) to describe the spectral features of **BisSQ2-AggI**.[6a,15] With the additional ICT states, the experimental absorption spectrum can be adequately reproduced (Figure 6c, blue solid line) with the parameters being in line with previous studies for thin films of squaraine dyes[15] (Table S2). We are aware that the chosen dimer unit does not account for all *inter*chromophoric interactions within the aggregate, so that the calculated spectrum had to be shifted by 200 cm^{-1} to higher energies to match the experimental spectrum. Therefore, the coupling strengths should be regarded as effective parameters to describe the absorption features of the tubular **BisSQ2-AggI** nanorod. However, the band shape is well reproduced by our simulations.

Further analysis reveals that mainly two transitions are present when vibronic coupling is neglected, causing the high and low energy absorption band at ≈620 and ≈780 nm, respectively (Figure S19, orange solid line). Hence, we can attribute the additionally observed absorption band at ≈730 nm to a vibronic band, which is caused by structural changes of the chromophores in the *intra*- and *inter*molecular charge transfer states with respect to the neutral state. In order to elucidate the influence of the *inter*molecular CT coupling strength t_{CT} on the absorption properties, which reflects the strength of the donor-acceptor interaction between the two chromophores, we have also calculated the spectra for different coupling strengths. For weak coupling ($t_{CT} = 1000$ cm^{-1}), which equals a small donor-acceptor overlap between the chromophores, the spectrum is characterized by one main absorption band (Figure S20, red dashed line). However, upon increasing the coupling strength up to 3000 cm^{-1} (note that we have used a value of $t_{CT} = 2550$ cm^{-1} to obtain best agreement with the experimental spectrum of **BisSQ2-AggI**), a two-band structure evolves with increasing energetic separation between the two absorption maxima (Figure S20, green and black solid line).

These results clearly show that the pronounced donor-acceptor overlap within **BisSQ2-AggI** nanorods is responsible for the panchromatic absorption band observed in the UV/Vis/NIR spectrum, which significantly differs from the predictions based on conventional molecular exciton theory.

In addition, we have also simulated the absorption spectrum of **BisSQ2-AggII**, which also shows a significant donor-acceptor overlap but now with a head-to-tail arrangement of the chromophores (Figure 3d). Indeed, the simulated spectrum (Figure 6d, blue solid line) shows a red-shift of the main absorption band as expected for chromophores showing J-type coupling.[18] Note that the simulated spectrum was additionally shifted by 500 cm^{-1} to lower energies in order to adjust the position of the main absorption peak with the experimental spectrum. We attribute the required correction of the absorption maximum to the chosen system size (dimer), so that only the interaction with one chromophore is considered and next-neighbor couplings are neglected, which should cause a stronger bathochromic shift. In addition, our simulations do not account for the J-type coupling between the two chromophores within the same **BisSQ2** molecule that causes an additional bathochromic shift (Figure S1c). Notably, when only Coulomb coupling is considered, the absorption shows a weaker bathochromic shift (Figure S21, red solid line) compared to the spectrum when also ICT states are considered (blue solid line). This indicates that the pronounced bathochromic shift for **BisSQ2-AggII** is caused by an interplay of Coulomb coupling and donor-acceptor interaction. Thus, whereas the donor-acceptor interaction in a sandwich-type arrangement of the squaraine chromophores induces the panchromatic absorption as observed for **BisSQ2-AggI** (Figure 6c, blue line), it leads to an increase of the bathochromic shift in the case of slip-stacked arranged chromophores like for **BisSQ2-AggII** (Figure 6d, blue solid line).

Conclusion

In this work, we studied the self-assembly of a new bis(squaraine) dye, in which two chromophores are covalently linked by a *para*-phenylene spacer moiety. In the low polarity solvent mixture toluene/TCE (98:2, *v*/*v*), **BisSQ2** self-assembles cooperatively into two different supramolecular polymorphs with very distinct structures and absorption spectra depending on the cooling rate. Rapid cooling results in structurally defined rigid helical nanorods with a diameter of ≈5 nm and a helical pitch of ≈13 nm (**BisSQ2-AggI**) while slow cooling gives rise to a nanosheet structure with a height of ≈2 nm (**BisSQ2-AggII**). The self-assembly processes can be well interpreted in terms of the cooperative K_2/K model, revealing a cooperativity factor of $\sigma = 0.016$ and binding constants for the nucleation of $K_2 = 3.56 \times 10^3$ M^{-1} and for the elongation of $K = 2.18 \times 10^5$ M^{-1} for **BisSQ2-AggI**, and $\sigma = 0.00038$, $K_2 = 2.42 \times 10^2$ M^{-1} and $K = 6.37 \times 10^5$ M^{-1} in the case of **BisSQ2-AggII**. With this information, we were able to derive a qualitative energy landscape (Figure 5) that illustrates the kinetically favored formation of **BisSQ2-AggI** and the thermodynamically favored formation of **BisSQ2-AggII**. A second important aspect of this work arises from the crystal-like well-defined packing of **BisSQ2** dyes in the two polymorphic aggregates **BisSQ2-AggI** and **BisSQ2-AggII**. Thus, packing arrangements could be derived from microscopic observations and X-ray scattering for both the thermodynamically stable **BisSQ2-AggII** nanosheets and the tubular **BisSQ2-AggI** nanorods. These structural models could be utilized in a subsequent step to elucidate the impact of packing on the UV/Vis/NIR absorption spectra of these dye aggregates. Whilst the conventional molecular exciton model failed to explain the absorption properties of **BisSQ2-AggI** for the given packing arrangement, more profound theoretical investigations based on the Essential States Model reveal the importance of *inter*molecular charge transfer to adequately describe the panchromatic broad absorption in the **BisSQ2-AggI** absorption spectrum. Moreover, the pronounced red-shift observed in the **BisSQ2-AggII** absorption spectrum can be assigned to the interplay of Coulomb coupling and *inter*molecular charge transfer.

In summary, we herein presented a supramolecular polymorphism for the self-assembly of a bis(squaraine) dye leading to unique highly defined nanosheets and tubular dye nanorods whose very different absorption spectra could be related to differences in the donor-acceptor overlap.

Beyond the importance of our results for research on supramolecular polymers and dye aggregates, we consider our insights on short-range charge transfer coupling for squaraine dyes with their donor-acceptor-donor structure to be of high relevance for all materials based on alternating donor-acceptor π-systems. This includes in particular acceptor-donor-acceptor (ADA) dyes that are currently the favored class of materials for bulk heterojunction solar cells.[37]

Acknowledgements

We thank the Bavarian State Ministry of Education, Science and the Arts for generous support for the newly established Key Laboratory for Supramolecular Polymers at the Center for Nanosystems Chemistry. K.S. thanks the Alexander von Humboldt foundation for a Bessel Award that supported a research stay in Germany. Open access funding enabled and organized by Projekt DEAL.

Conflict of interest

The authors declare no conflict of interest.

Keywords: cooperative self-assembly · nanorods and nanosheets · polymorphism · squaraine dyes · supramolecular polymers

[1] a) F. Würthner, T. E. Kaiser, C. R. Saha-Möller, *Angew. Chem. Int. Ed.* **2011**, *50*, 3376 – 3410; *Angew. Chem.* **2011**, *123*, 3436 – 3473; b) N. J. Hestand, F. C. Spano, *Chem. Rev.* **2018**, *118*, 7069 – 7163; c) W. Herbst, K. Hunger, *Industrial Organic Pigments: Production, Properties, Applications*, 3rd, Completely Revised ed., Wiley-VCH, Weinheim, **2004**.

[2] J. Bernstein, *Polymorphism in Molecular Crystals*, Oxford University Press, Oxford, **2010**.

[3] P. Erk, H. Hengelsberg, M. F. Haddow, R. van Gelder, *CrystEngComm* **2004**, *6*, 474 – 483.

[4] M. Gsänger, D. Bialas, L. Huang, M. Stolte, F. Würthner, *Adv. Mater.* **2016**, *28*, 3615 – 3645.

[5] a) T. Fukui, S. Kawai, S. Fujinuma, Y. Matsushita, T. Yasuda, T. Sakurai, S. Seki, M. Takeuchi, K. Sugiyasu, *Nat. Chem.* **2017**, *9*, 493 – 499; b) N. M. Matsumoto, R. P. M. Lafleur, X. Lou, K.-C. Shih, S. P. W. Wijnands, C. Guibert, J. W. A. M. van Rosendaal, I. K. Voets, A. R. A. Palmans, Y. Lin, E. W. Meijer, *J. Am. Chem. Soc.* **2018**, *140*, 13308 – 13316; c) A. Langenstroer, K. K. Kartha, Y. Dorca, J. Droste, V. Stepanenko, R. Q. Albuquerque, M. R. Hansen, L. Sánchez, G. Fernández, *J. Am. Chem. Soc.* **2019**, *141*, 5192 – 5200; d) M. Wehner, M. I. S. Röhr, M. Bühler, V. Stepanenko, W. Wagner, F. Würthner, *J. Am. Chem. Soc.* **2019**, *141*, 6092 – 6107; e) N. Sasaki, M. F. J. Mabesoone, J. Kikkawa, T. Fukui, N. Shioya, T. Shimoaka, T. Hasegawa, H. Takagi, R. Haruki, N. Shimizu, S. Adachi, E. W. Meijer, M. Takeuchi, K. Sugiyasu, *Nat. Commun.* **2020**, *11*, 3578; f) E. E. Greciano, J. Calbo, E. Ortí, L. Sánchez, *Angew. Chem. Int. Ed.* **2020**, *59*, 17517 – 17524; *Angew. Chem.* **2020**, *132*, 17670 – 17677; g) M. Hecht, P. Leowanawat, T. Gerlach, V. Stepanenko, M. Stolte, M. Lehmann, F. Würthner, *Angew. Chem. Int. Ed.* **2020**, *59*, 17084 – 17090; *Angew. Chem.* **2020**, *132*, 17232 – 17238; h) J. Matern, K. K. Kartha, L. Sánchez, G. Fernández, *Chem. Sci.* **2020**, *11*, 6780 – 6788; i) I. Helmers, B. Shen, K. K. Kartha, R. Q. Albuquerque, M. Lee, G. Fernández, *Angew. Chem. Int. Ed.* **2020**, *59*, 5675 – 5682; *Angew. Chem.* **2020**, *132*, 5724 – 5731; j) T. Aizawa, K. Aratsu, S. Datta, T. Mashimo, T. Seki, T. Kajitani, F. Silly, S. Yagai, *Chem. Commun.* **2020**, *56*, 4280 – 4283.

[6] For polymorphism studies in the field of squaraine thin films and crystals, see: a) M. Tristani-Kendra, C. J. Eckhardt, *J. Chem. Phys.* **1984**, *81*, 1160 – 1173; b) A. Viterisi, N. F. Montcada, C. V. Kumar, F. Gispert-Guirado, E. Martin, E. Escudero, E. Palomares, *J. Mater. Chem. A* **2014**, *2*, 3536 – 3542; c) F. Balzer, H. Kollmann, M. Schulz, G. Schnakenburg, A. Lützen, M. Schmidtmann, C. Lienau, M. Silies, M. Schiek, *Cryst. Growth Des.* **2017**, *17*, 6455 – 6466; d) J. Zablocki, O. Arteaga, F. Balzer, D. Hertel, J. J. Holstein, G. Clever, J. Anhäuser, R. Puttreddy, K. Rissanen, K. Meerholz, A. Lützen, M. Schiek, *Chirality* **2020**, *32*, 619 – 631.

[7] a) L. Gisslén, R. Scholz, *Phys. Rev. B* **2009**, *80*, 115309; b) N. J. Hestand, F. C. Spano, *J. Chem. Phys.* **2015**, *143*, 244707; c) B. Engels, V. Engel, *Phys. Chem. Chem. Phys.* **2017**, *19*, 12604 – 12619; d) C. Kaufmann, D. Bialas, M. Stolte, F. Würthner, *J. Am. Chem. Soc.* **2018**, *140*, 9986 – 9995; e) A. Oleson, T. Zhu, I. S. Dunn, D. Bialas, Y. Bai, W. Zhang, M. Dai, D. R. Reichman, R. Tempelaar, L. Huang, F. C. Spano, *J. Phys. Chem. C* **2019**, *123*, 20567 – 20578; f) M. Hecht, F. Würthner, *Acc. Chem. Res.* **2021**, *54*, 642 – 653.

[8] S. Sreejith, P. Carol, P. Chithra, A. Ajayaghosh, *J. Mater. Chem.* **2008**, *18*, 264 – 274.

[9] L. Beverina, P. Salice, *Eur. J. Org. Chem.* **2010**, 1207 – 1225.

[10] M. Gsänger, E. Kirchner, M. Stolte, C. Burschka, V. Stepanenko, J. Pflaum, F. Würthner, *J. Am. Chem. Soc.* **2014**, *136*, 2351 – 2362.

[11] a) U. Mayerhöffer, K. Deing, K. Gruss, H. Braunschweig, K. Meerholz, F. Würthner, *Angew. Chem. Int. Ed.* **2009**, *48*, 8776 – 8779; *Angew. Chem.* **2009**, *121*, 8934 – 8937; b) K. C. Deing, U. Mayerhöffer, F. Würthner, K. Meerholz, *Phys. Chem. Chem. Phys.* **2012**, *14*, 8328 – 8334; c) X. Xiao, G. D. Wei, S. Y. Wang, J. D. Zimmerman, C. K. Renshaw, M. E. Thompson, S. R. Forrest, *Adv. Mater.* **2012**, *24*, 1956 – 1960; d) T. Maeda, T. Tsukamoto, A. Seto, S. Yagi, H. Nakazumi, *Macromol. Chem. Phys.* **2012**, *213*, 2590 – 2597; e) G. Chen, H. Sasabe, W. Lu, X.-F. Wang, J. Kido, Z. Hong, Y. Yang, *J. Mater. Chem. C* **2013**, *1*, 6547 – 6552.

[12] a) M. Schulz, M. Mack, O. Kolloge, A. Lützen, M. Schiek, *Phys. Chem. Chem. Phys.* **2017**, *19*, 6996 – 7008; b) M. Schulz, J. Zablocki, O. S. Abdullaeva, S. Brück, F. Balzer, A. Lützen, O. Arteaga, M. Schiek, *Nat. Commun.* **2018**, *9*, 2413.

[13] J. J. Gassensmith, J. M. Baumes, B. D. Smith, *Chem. Commun.* **2009**, 6329 – 6338.

[14] a) R. S. Stoll, N. Severin, J. P. Rabe, S. Hecht, *Adv. Mater.* **2006**, *18*, 1271 – 1275; b) K. Jyothish, M. Hariharan, D. Ramaiah, *Chem. Eur. J.* **2007**, *13*, 5944 – 5951; c) P. Chithra, R. Varghese, K. P. Divya, A. Ajayaghosh, *Chem. Eur. J.* **2008**, *14*, 1365 – 1373; d) U. Mayerhöffer, F. Würthner, *Chem. Sci.* **2012**, *3*, 1215 – 1220; e) U. Mayerhöffer, F. Würthner, *Angew. Chem. Int. Ed.* **2012**, *51*, 5615 – 5619; *Angew. Chem.* **2012**, *124*, 5713 – 5717; f) Y. Zhang, B. Kim, S. Yao, M. V. Bondar, K. D. Belfield, *Langmuir* **2013**, *29*, 11005 – 11012.

[15] N. J. Hestand, C. Zheng, A. R. Penmetcha, B. Cona, J. A. Cody, F. C. Spano, C. J. Collison, *J. Phys. Chem. C* **2015**, *119*, 18964 – 18974.

[16] a) S. Ito, P. T. Herwig, T. Böhme, J. P. Rabe, W. Rettig, K. Müllen, *J. Am. Chem. Soc.* **2000**, *122*, 7698 – 7706; b) F. Würthner, S. Yao, U. Beginn, *Angew. Chem. Int. Ed.* **2003**, *42*, 3247 – 3250; *Angew. Chem.* **2003**, *115*, 3368 – 3371; c) S. Yagai, S. Kubota, T. Iwashima, K. Kishikawa, T. Nakanishi, T. Karatsu, A. Kitamura, *Chem. Eur. J.* **2008**, *14*, 5246 – 5257; d) M. Yamauchi, Y. Chiba, T. Karatsu, A. Kitamura, S. Yagai, *Chem. Lett.* **2013**, *42*, 799 – 800; e) X. Lin, Y. Okazawa, Y. Tani, H. Ouchi, K. Nakayama, S. Yagai, *Asian J. Org. Chem.* **2020**, *9*, 222 – 225.

[17] C.-A. Shen, F. Würthner, *Chem. Commun.* **2020**, *56*, 9878 – 9881.

[18] M. Kasha, H. R. Rawls, M. A. El-Bayoumi, *Pure Appl. Chem.* **1965**, *11*, 371 – 392.
[19] a) A. Painelli, F. Terenziani, *J. Phys. Chem. A* **2000**, *104*, 11041 – 11048; b) F. Terenziani, A. Painelli, *Phys. Rev. B Condens. Matter Mater. Phys.* **2003**, *68*, 165405.
[20] a) M. I. S. Röhr, H. Marciniak, J. Hoche, M. H. Schreck, H. Ceymann, R. Mitrić, C. Lambert, *J. Phys. Chem. C* **2018**, *122*, 8082 – 8093; b) C. Zhong, D. Bialas, C. J. Collison, F. C. Spano, *J. Phys. Chem. C* **2019**, *123*, 18734 – 18745.
[21] a) F. Würthner, *Acc. Chem. Res.* **2016**, *49*, 868 – 876; b) S. Yagai, *Bull. Chem. Soc. Jpn.* **2015**, *88*, 28 – 58.
[22] M. Wehner, M. I. S. Röhr, V. Stepanenko, F. Würthner, *Nat. Commun.* **2020**, *11*, 5460.
[23] It is noteworthy that the appearance of helical structures for such supramolecular polymers is quite common. Accordingly, the situation for one-dimensional structures is different from three-dimensional crystals where conglomerates are the exceptions and racemic crystals the more general case, see: A. Palmans, *Mol. Syst. Des. Eng.* **2017**, *2*, 34 – 46.
[24] S. Herbst, B. Soberats, P. Leowanawat, M. Lehmann, F. Würthner, *Angew. Chem. Int. Ed.* **2017**, *56*, 2162 – 2165; *Angew. Chem.* **2017**, *129*, 2194 – 2197.
[25] W. Zhang, W. Jin, T. Fukushima, N. Ishii, T. Aida, *Angew. Chem. Int. Ed.* **2009**, *48*, 4747 – 4750; *Angew. Chem.* **2009**, *121*, 4841 – 4844.
[26] M. M. J. Smulders, M. M. L. Nieuwenhuizen, T. F. A. de Greef, P. van der Schoot, A. P. H. J. Schenning, E. W. Meijer, *Chem. Eur. J.* **2010**, *16*, 362 – 367.
[27] T. E. Kaiser, V. Stepanenko, F. Würthner, *J. Am. Chem. Soc.* **2009**, *131*, 6719 – 6732.
[28] F. Fennel, S. Wolter, Z. Xie, P.-A. Plötz, O. Kühn, F. Würthner, S. Lochbrunner, *J. Am. Chem. Soc.* **2013**, *135*, 18722 – 18725.
[29] S. Ogi, T. Fukui, M. L. Jue, M. Takeuchi, K. Sugiyasu, *Angew. Chem. Int. Ed.* **2014**, *53*, 14363 – 14367; *Angew. Chem.* **2014**, *126*, 14591 – 14595.
[30] L. Yang, G. Fan, X. Ren, L. Zhao, J. Wang, Z. Chen, *Phys. Chem. Chem. Phys.* **2015**, *17*, 9167 – 9172.
[31] C. M. A. Leenders, L. Albertazzi, T. Mes, M. M. E. Koenigs, A. R. A. Palmans, E. W. Meijer, *Chem. Commun.* **2013**, *49*, 1963 – 1965.
[32] a) E. E. Jelley, *Nature* **1936**, *138*, 1009 – 1010; b) G. Scheibe, *Angew. Chem.* **1937**, *50*, 212 – 219.
[33] A. Austin, N. J. Hestand, I. G. McKendry, C. Zhong, X. Zhu, M. J. Zdilla, F. C. Spano, J. M. Szarko, *J. Phys. Chem. Lett.* **2017**, *8*, 1118 – 1123.
[34] B. Bardi, C. Dall'Agnese, K. I. Moineau-Chane Ching, A. Painelli, F. Terenziani, *J. Phys. Chem. C* **2017**, *121*, 17466 – 17478.
[35] C. Zheng, C. Zhong, C. J. Collison, F. C. Spano, *J. Phys. Chem. C* **2019**, *123*, 3203 – 3215.
[36] S. Sanyal, A. Painelli, S. K. Pati, F. Terenziani, C. Sissa, *Phys. Chem. Chem. Phys.* **2016**, *18*, 28198 – 28208.
[37] C. Yan, S. Barlow, Z. Wang, H. Yan, A. K.-Y. Jen, S. R. Marder, X. Zhan, *Nat. Rev. Mater.* **2018**, *3*, 18003.

Manuscript received: February 11, 2021
Accepted manuscript online: March 10, 2021
Version of record online: May 1, 2021

